Supporting Information for

Monitoring Food Spoilage Biogenic Amines Utilizing a Blue-Emitting Fluorescent Ionic Liquid

Najmin Tohora[a], Biswajit Bhaumik[a], Rajkumar Sahoo[b], and Sudhir Kumar Das[a*]

[a]Department of Chemistry, University of North Bengal, Raja Rammohunpur, Darjeeling, West Bengal-734013, India

[b]Department of Chemistry, Indian Institute of Technology, Kharagpur 721302, India

Corresponding author: (Dr. S. K. Das; E-mail: sudhirkumardas@nbu.ac.in)

S1. Experimental sections

S1.1 General Method & Instrumentations

Chemical reagents are purchased from Sigma Aldrich, India, and used without further purification. Anhydrous solvents and HPLC spectroscopic grade were obtained from Merck, India. 9, 10-phenanthrenequinone, 1-naphthaldehyde and trihexyltetradecylphosphonium chloride ([TTP]Cl) are purchased from Sigma-Aldrich, India. All the metal salts, anions, and biologically relevant molecules used in the present study are purchased from Sigma-Aldrich, India, and TCI, India, respectively. Dimethyl sulphoxide (DMSO-d_6) is obtained from Sigma Aldrich, India, and is used for the NMR spectral analysis. Quatro Micro API (MICROMASS, UK), lc-WATERS 2695 spectrometer having detector PDA2998, ESI_Negative with capillary voltage 3 kV, Cone -30 V and extractor-3 V employing source and dissolving temperature -90℃ and -250℃ respectively using dissolving gas-450 Litre/hour with flow rate-10 μL/min. UV-visible spectral studies are carried out on a HITACHI U-2910, and fluorescence experiments are carried out on a HITACHI F-7100 fluorimeter with a 5 nm excitation and emission slit, respectively. Throughout the steady-state emission experiment, excitation and emission wavelengths are maintained at 370 nm and 390-720 nm, respectively.

The size and shape of the **nTPND** are estimated by field emission scanning electron microscopy (SEM) (ZEISS) employing an operating voltage of 50 kV by drop casting the required amounts of **nTPND** on the carbon-coated copper grids. The average particle size is determined by considering the size of more than 100 particles. The hydrodynamic radius of **nTPND** is measured employing the dynamic light scattering (DLS) technique (Anton Paar Litesizer 500), and the PDI of the DLS measurements is 27.8% or 0.278. The zeta potential (ζ) of nanoparticles is also obtained by this instrument using a capillary ζ-cell.

S1.2 General procedure for UV–visible and fluorescence Experiments

The stock solutions of the probe, **nTPND** (12 μM), metal chloride solutions (10^{-3} M), sodium & potassium salts of anions (10^{-3} M), and biologically relevant molecules (10^{-3} M) were prepared in aqueous solution. The fluorescence response of various metal ions (Mn^{2+}, Ni^{2+}, Zn^{2+}, Na^{+}, K^{+}, Cu^{2+}, Fe^{3+}, Al^{3+}, Cr^{3+}), anions ($H_2PO_4^-$, NO_3^-, OAc^-, SO_4^{2-}, CO_3^{2-}, Br^-, Cl^-, I^-), small molecules and reagents (NH_3, H_2O_2, ethylenediaminetetraacetic acid **(**EDTA)) and biologically relevant amines (putrescine (PUT), dopamine (DOP), histidine (HIS)) alongside SPM and SPD were investigated. The probe's selectivity has been tested against all metal ions, anions, small molecules, reagents, and biologically relevant molecules using fluorescence and colorimetric experiments. Fluorescence and UV-visible titrations were performed using varying concentrations of metal ions, biologically relevant molecules, and anion solutions. To determine the σ value, we have recorded ten absorption /photoluminescence spectra of **nTPND** solution without SPD and SPM, and the standard deviation is estimated, which is used to determine the LOD value.

S1.3 Preparation of portable paper-based test strips

The Whatman-41 filter paper is cut into strips, which are fully immersed in **nTPND** aqueous solution (12 μM) for a while. Finally, the test strips are removed and dried in a hot

air oven. Some drops of all metal ions, anions, small molecules, reagents, and biologically relevant molecules (10^{-3} M) are added to these filter papers.

S1.4 Experimental protocol for mushroom-based vapor-phase detection of SPD/SPM

Fresh mushrooms were purchased locally and used for the experiment. 10 gm of the mushroom sample was gently rinsed with distilled water to remove surface impurities and loosely bound contaminants, and then air-dried before use. The mushroom was placed in a sterile round-bottom flask, which was connected via an L-connector to a conical flask containing 2 mg of neat **TPND**. The entire setup was maintained at room temperature under ambient conditions.

S1.5 Protocol for soil and water sample analysis

For the soil sample experiment, 0.5 g of soil was spiked with 10^{-3} M SPD/SPM, followed by the addition of aqueous **nTPND** dispersion (12 μM) and gentle mixing. The mixture was allowed to settle for 5 mins, and the supernatant was used for fluorescence measurements. For water sample analysis, we have collected water samples from different parts of Siliguri, India, and spiked them with 10^{-3} M SPD. In each sample of 2 mL volume (12 μM), a different quantity of SPD with acquainted concentrations is added, and changes in fluorescence intensity are recorded.

S1.6 Measurement of fluorescence quantum yield

For the estimation of fluorescence quantum yield, we have considered the quinine sulfate as a standard in 1(N) H_2SO_4 (Φ=0.546) [1]. Using the equation $: \Phi = \Phi_s\left(\frac{F_x}{F_s}\right)\left(\frac{A_s}{A_x}\right)\left(\frac{{\eta_x}^2}{{\eta_s}^2}\right)$, where Φ stands for quantum yield, F is the integrated fluorescence intensity, A is the absorbance, η defines the refractive index of the solvent, subscript 's' defines the standard quinine sulfate, and x is the unknown one, we have calculated the quantum yield (Φ) of **TPND**, **nTPND, nTPND-SPD, and nTPND-SPM,** respectively.

Characterization of NPI: (^{1}H NMR, DMSO-d_6, 400 MHz, in ppm units): 11.93 (s, 1H, NH), 8.93 (d, 2H), 8.55 (d, 1H), 8.12 (d, 2H), 8.08 (d, 1H), 8.04 (d, 1H), 7.95 (d, 1H), 7.88 (dd, 2H), 7.82 (dd, 2H), 7.61 (dd, 1H), 7.55 (d, 2H) (**Fig. S1**).

Characterization of compound SNPI: (^{1}H NMR, DMSO-d_6, 400 MHz, in ppm units): 8.90 (d, 2H), 8.38 (d, 1H), 8.32 (d, 1H), 8.10 (d, 2H), 8.08 (d, 1H), 7.93 (d, 1H), 7.9 (dd, 2H), 7.8 (dd, 2H), 7.79 (dd, 1H), 7.55 (d, 2H) (**Fig. S3**).

Characterization of TPND: (^{1}H NMR, DMSO-d_6, 400 MHz, in ppm units): 8.90 (d, 2H), 8.38 (d, 1H), 8.32 (d, 1H), 8.1 (d, 2H), 8.08 (d, 1H), 7.93 (d, 1H), 7.90 (dd, 2H), 7.80 (dd, 2H), 7.79 (dd, 1H), 7.55 (d, 2H), 2.22-0.88 (various m, 68 H) (**Fig. S5**). **^{31}P NMR** (400 MHz, DMSO-d_6, δ (ppm): 33.93 (**Fig. S8).**

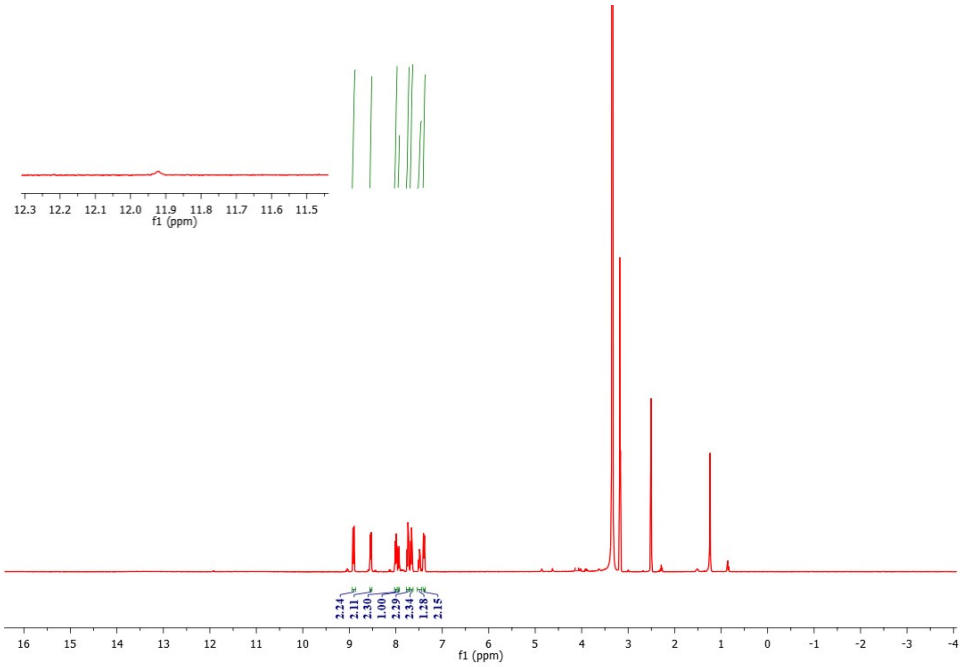

Fig. S1: ^{1}H NMR spectrum (DMSO-d_6, 400 MHz) of NPI.

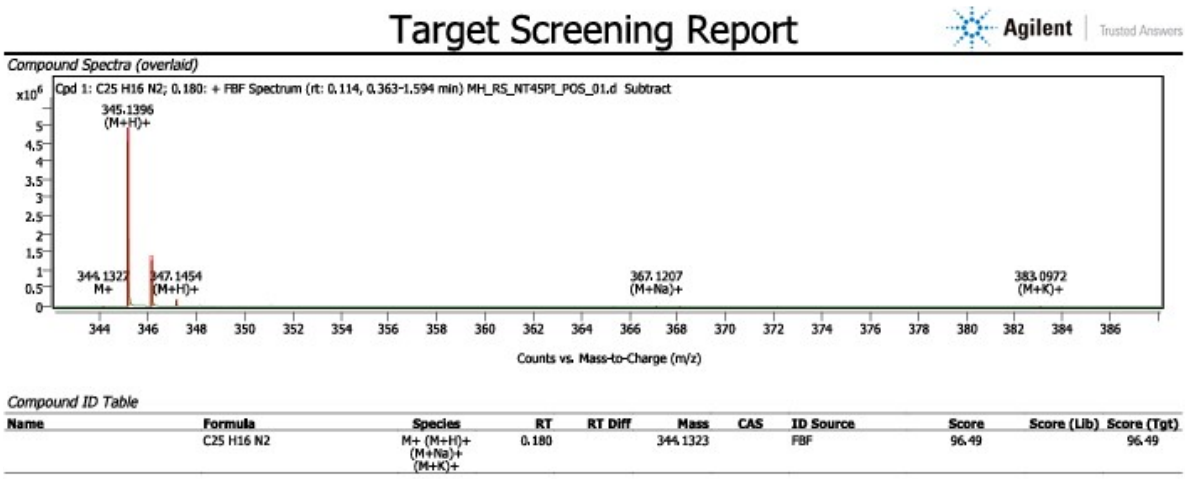

Fig. S2: HRMS spectra of NPI.

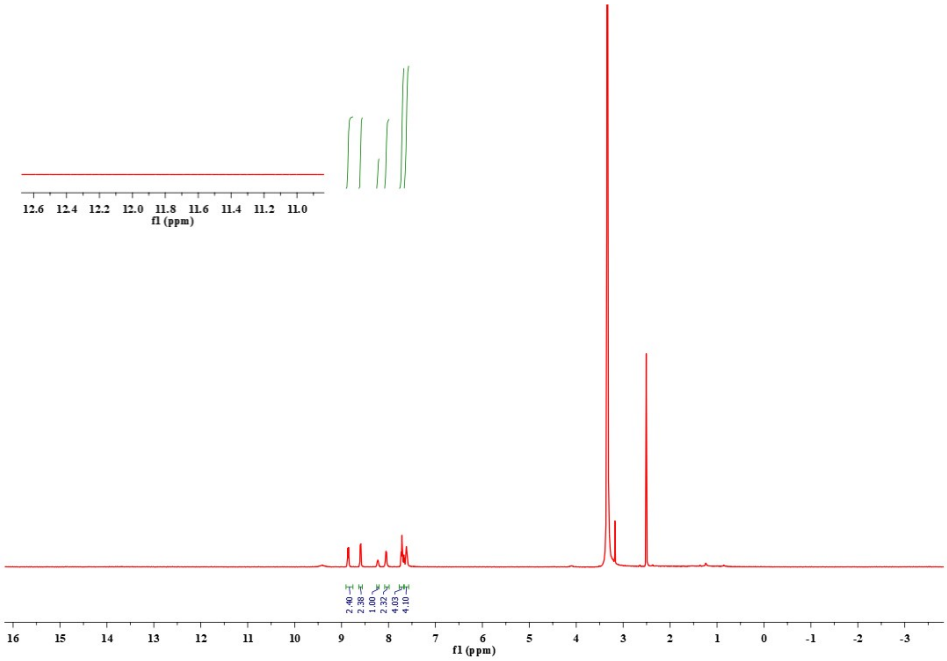

Fig. S3: ^{1}H NMR spectrum (DMSO-d_6, 400 MHz) of SNPI.

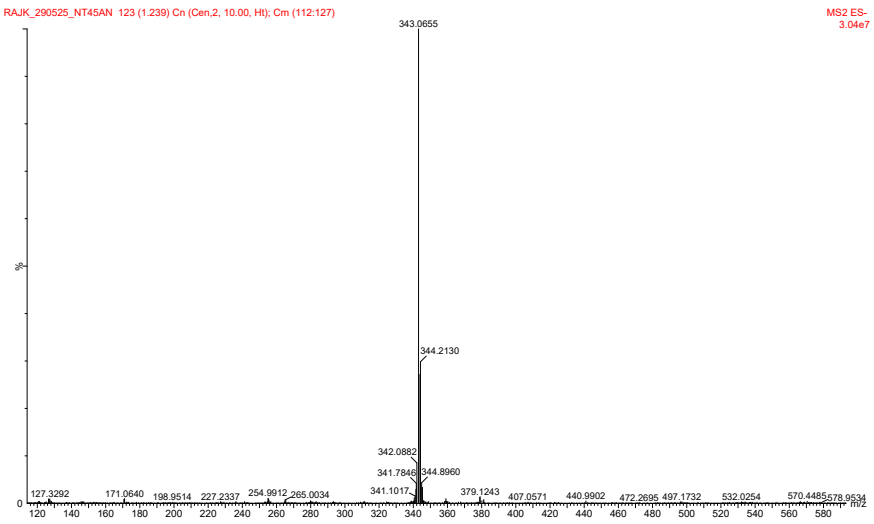

Fig. S4: LC-MS spectra of the negative component of SNPI.

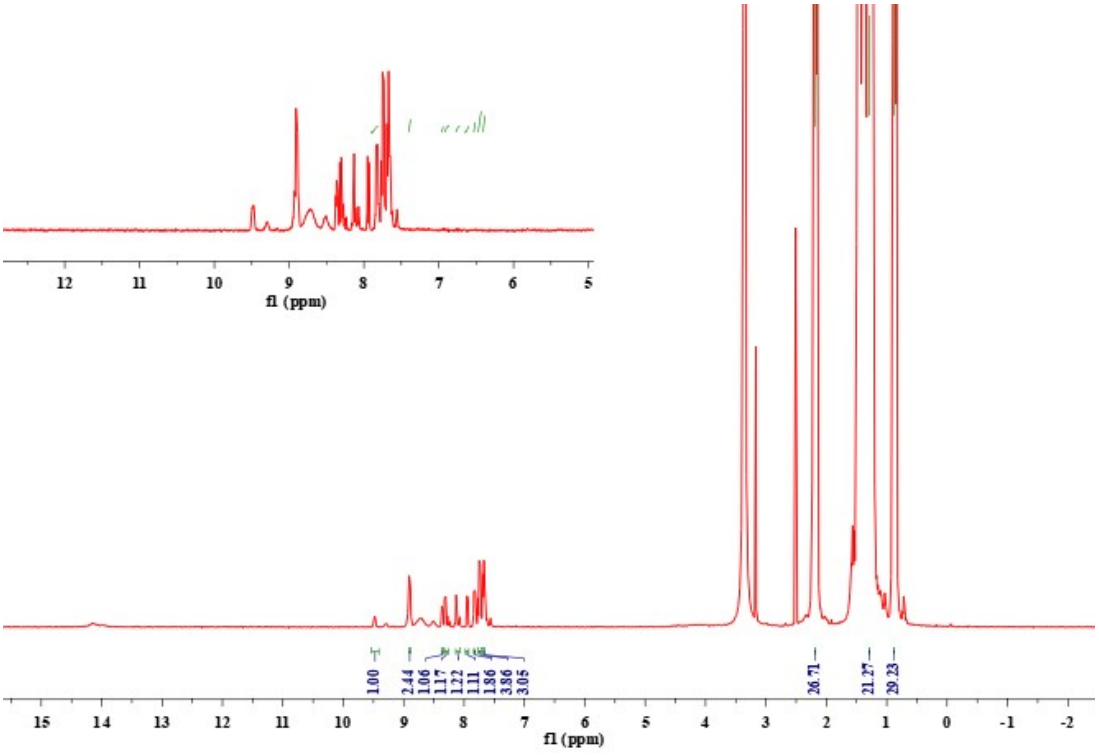

Fig. S5: ^{1}H NMR spectrum (DMSO-d_6, 400 MHz) of **TPND**.

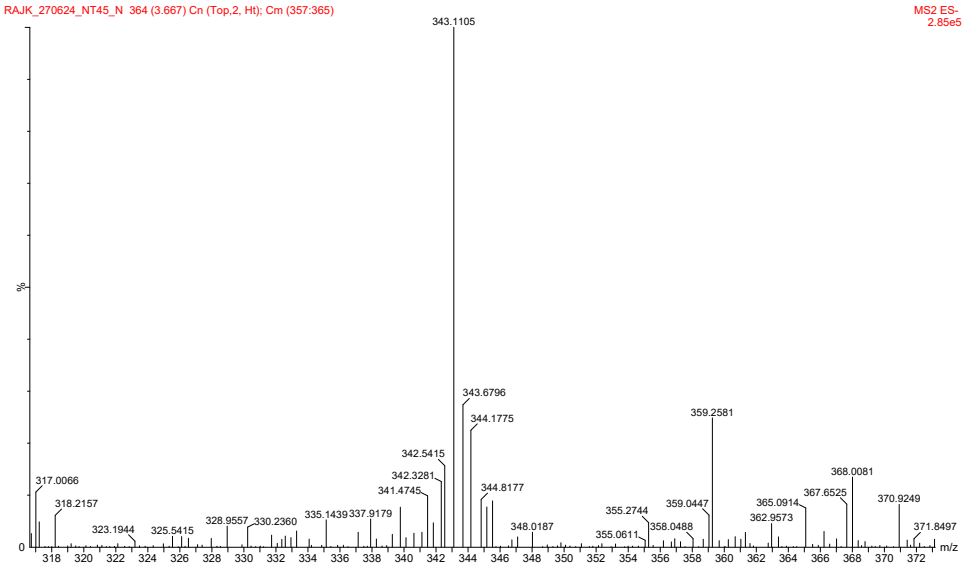

Fig. S6: LC-MS spectra of the negative component of **TPND**.

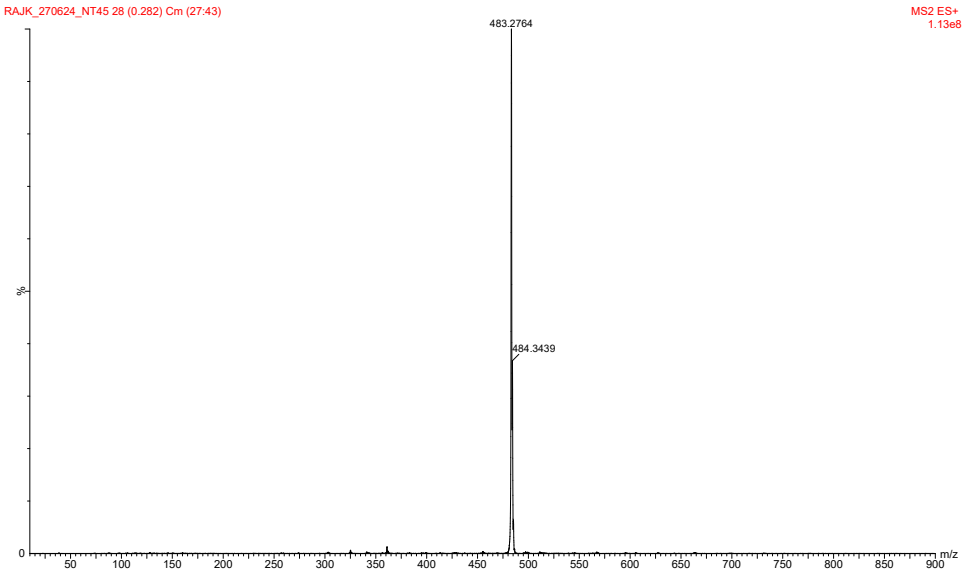

Fig. S7: LC-MS spectra of the positive component of **TPND**.

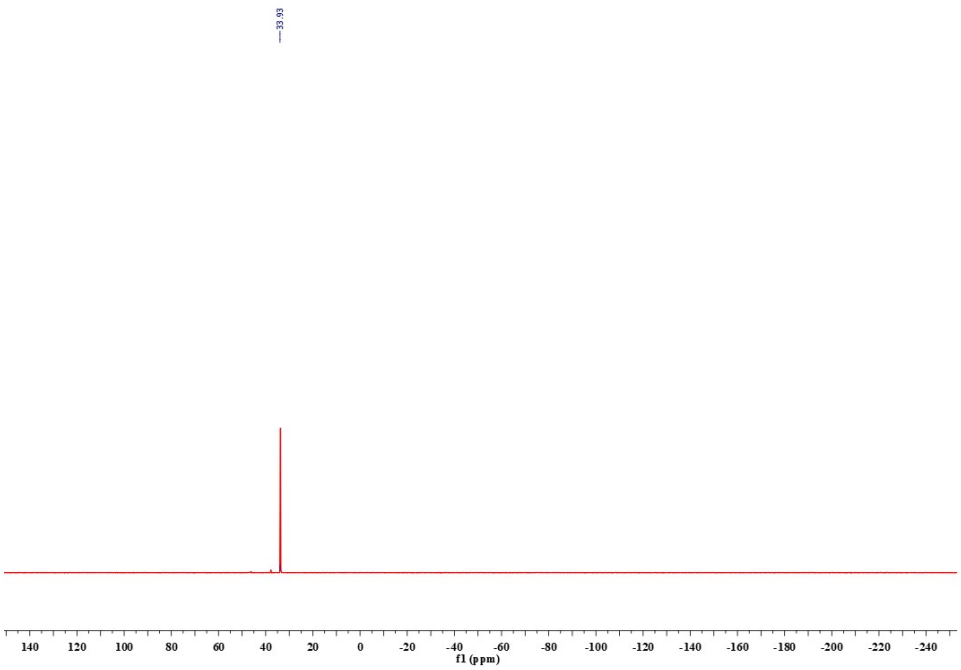

Fig. S8: ^{31}P NMR spectrum (DMSO-d_6, 400 MHz) of **TPND**.

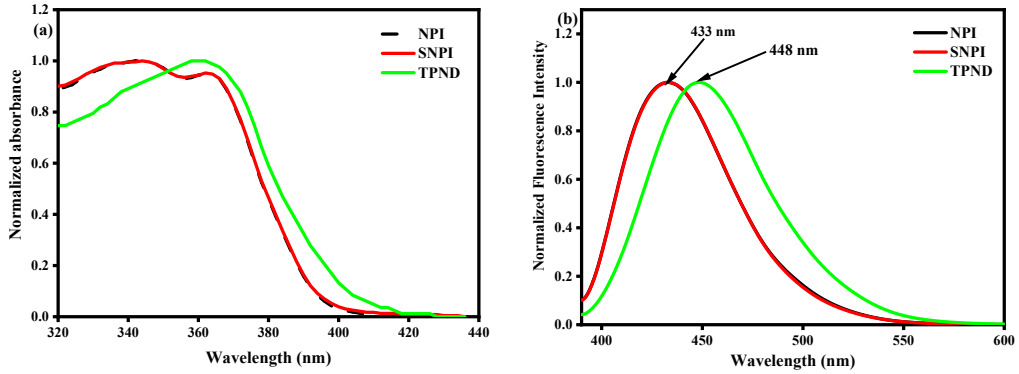

Fig. S9: (a) The normalized absorption spectra of NPI, SNPI, and **TPND** in DMSO. **(b)** The normalized fluorescence spectra of NPI, SNPI, and **TPND** in DMSO.

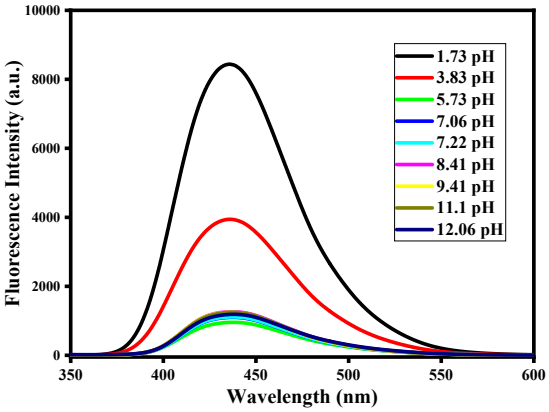

Fig. S10: The impact of pH on photoluminosity of NPI at 25 °C.

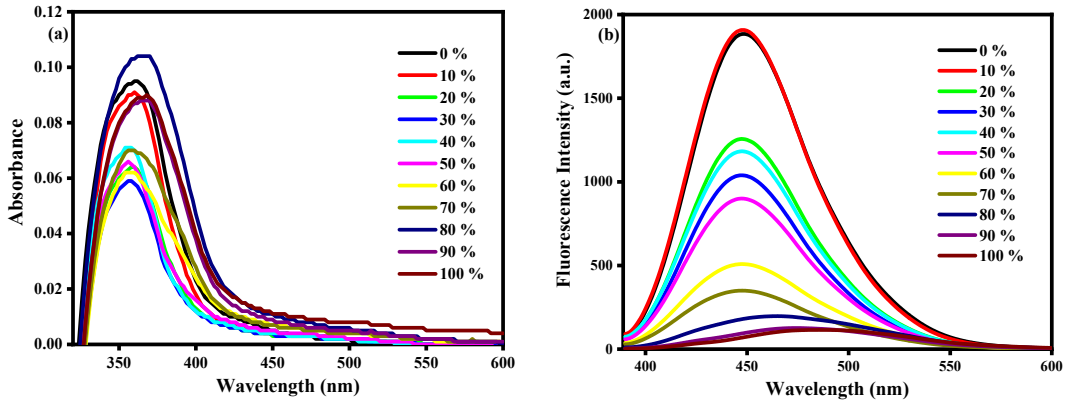

Fig. S11: (a) UV-vis absorption spectra of **TPND** in different percentages of water. **(b)** Fluorescence spectra of **TPND** in water-DMSO mixed solvents demonstrating ACQ.

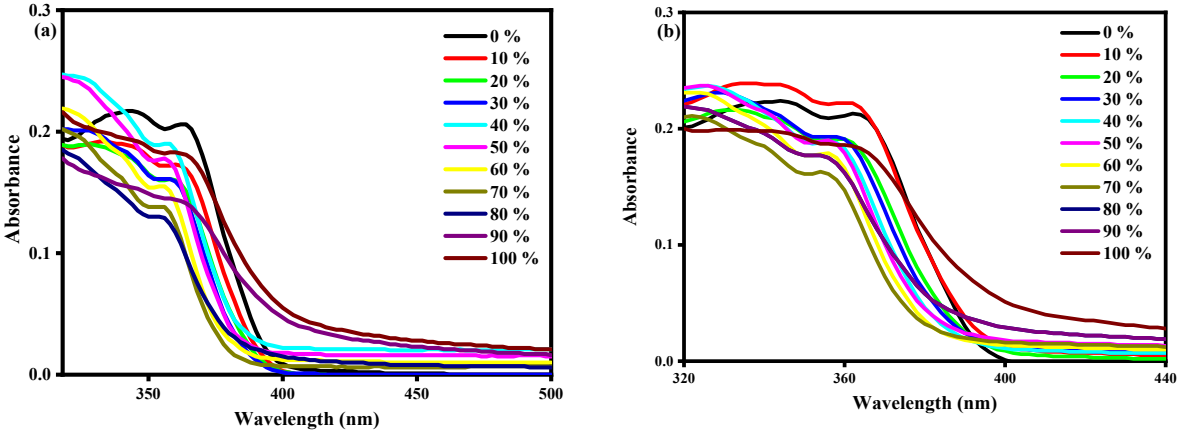

Fig. S12: (a) UV-vis absorption spectra of NPI in different percentages of water. **(b)** UV-vis absorption spectra of SNPI in different percentages of water.

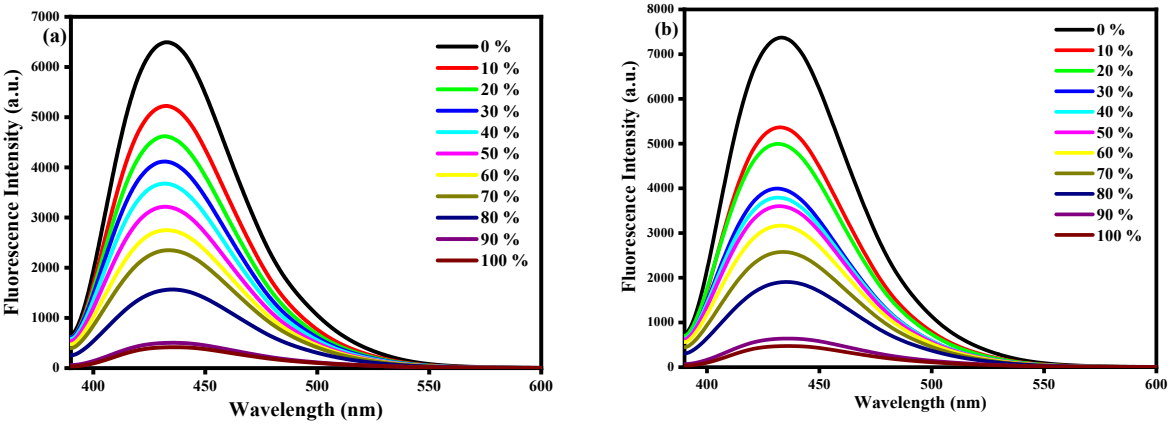

Fig. S13: (a) Fluorescence spectra of NPI in water-DMSO mixed solvents. **(b)** Fluorescence spectra of SNPI in water-DMSO mixed solvents.

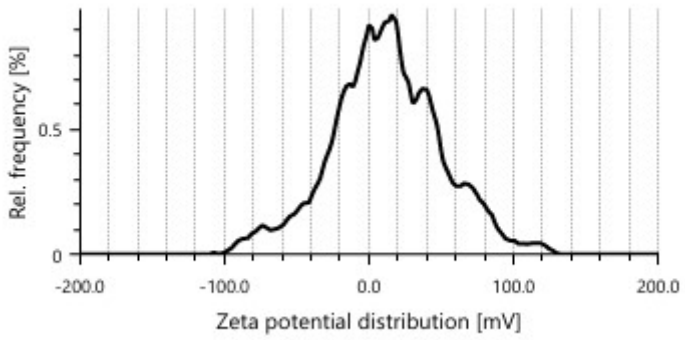

Fig. S14: The relative frequency vs. zeta potential distribution curve for the determination of the zeta potential of **nTPND**.

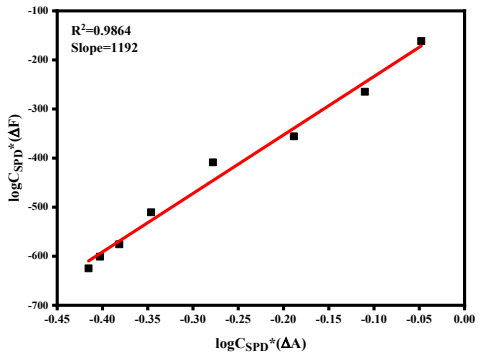

Fig. S15: Correlation of SPD detection results for fluorescent and colorimetric channels.

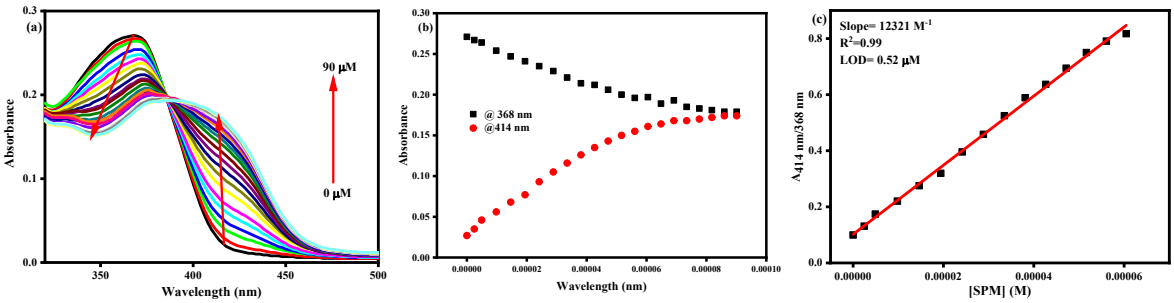

Fig. 16: (**a**) UV-vis absorption titration profiles for **nTPND** with incremental addition (0-90 μM) of SPM. (**b**) Plot of changes in absorbance intensity at $A_{368\ nm}$ and $A_{414\ nm}$ in **nTPND** solution versus [SPM]. **(c)** Limit of detection, determined from the linear relationship between the absorbance ratio ($A_{414\ nm}/A_{368\ nm}$) and SPM.

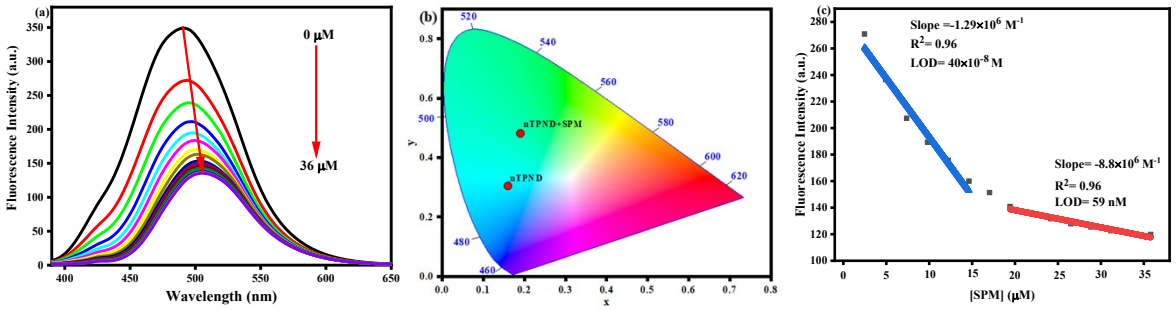

Fig. 17: (**a**) Photoluminescence intensity profile of **nTPND** in aqueous medium during progressive addition of SPM. **(b)** CIE chromaticity plot demonstrating the emission color shift from cyan to green. **(c)** Limit of detection, determined from the linear relationship between the fluorescence intensity at 482 nm and [SPM].

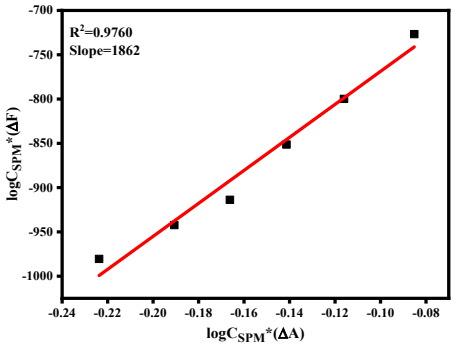

Fig. S18: Correlation of SPM detection results for fluorescent and colorimetric channels.

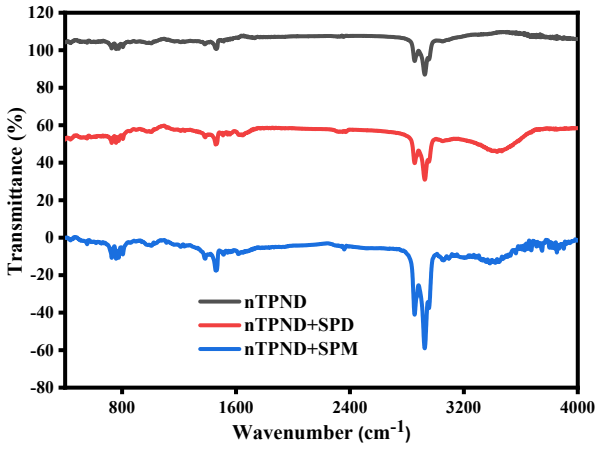

Fig. S19: IR spectra of **nTPND**, **nTPND**-SPD, and **nTPND**-SPM, respectively.

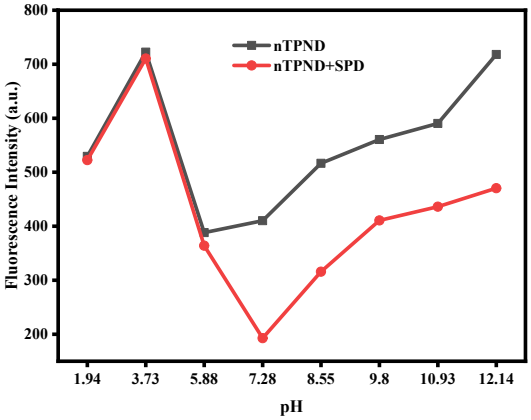

Fig. S20: The impact of pH on photoluminosity of **nTPND** with and without SPD at 25 °C.

Table S1. Absorption spectra in the UV-visible range and photoluminescence data of NPI were measured in different media and expressed in nanometers.

Solvents	Toluene (33.9) [a]	THF (37.4) [a]	DCM (40.7)	DMSO (45.1) [a]	H_2O (53.7) [a]
λ_{max}^{abs}	355	361	362	363	365
λ_{max}^{flu}	416	420	426	433	437

[a] Numbers in the first brackets represent the micro-polarity values [E_T (30)] [2] of the solvents. $\lambda_{exc.}$ = 350 nm.

Table S2. Absorption spectra in the UV-visible range and photoluminescence data of SNPI were measured in different media and expressed in nanometers.

Solvents	Toluene (33.9) [a]	THF (37.4) [a]	DCM (40.7)	DMSO (45.1) [a]	H_2O (53.7) [a]
λ_{max}^{abs}	358	360	362	363	364
λ_{max}^{flu}	416	419	427	433	437

[a] Numbers in the first brackets represent the micro-polarity values [E_T (30)] [2] of the solvents. $\lambda_{exc.}$ = 350 nm.

Table S3: Detection and quantification of SPM in different water samples.

Sample	Added (μM)	Found (μM)	Recovery (%)
River water	4.92	3.92	81.09
	9.80	8.50	86.73
	14.63	13.42	91.72

	19.41	18.54	95.51
	24.15	23.20	96.06
Tap water	4.92	4.28	86.99
	9.80	9.21	93.97
	14.63	12.87	87.96
	19.41	17.25	88.87
	24.15	23.11	95.69

Table S4: Evaluating the presence of SPD in spiked soil samples

Sample (Soil)	Added (µM)	Found (µM)	Recovery (%)
Clay	33	29.54	89.51

Table S5: Evaluating the presence of SPM in spiked soil samples

Sample (Soil)	Added (µM)	Found (µM)	Recovery (%)
Clay	33	26.54	80.42

Table S6. Comparison table for the detection of spermine and spermidine.

Materials	Analyte	LOD	Real sample	Ref
YQDs-BCDs	spermine/spermidine	0.2 µM/2.1 µM	Chicken and mutton meat.	[3]
Capped Silica Particles	spermine/spermidine	27 µM /45 µM	Urine	[4]
Tetraphenylethylene Derivative	spermine/spermidine	0.7 µM/1.17 µM	Urine	[5]
ratiometric fluorescent probe	spermine/spermidine	6.75 µM/3.85 µM	Raw shrimp	[6]
CuI-CP	spermine/spermidine/cysteine	0.57 µM/0.98 µM/1.18 µM	Pork samples	[7]
PTE + Cu^{2+}complex	spermine	0.6 µM	Fish, Cheese, and Mushroom	[8]
FID chemosensor based on TMeQ[6]	spermine/spermidine	0.0959 µM/0.0876 µM	Human urine and serum	[9]
ZnONPs-MWCNTs-CPE sensor	spermine	300 nM	Urine	[10]
Imidazolate-based	**Spermidine/spermine**	**36 nM/59 nM**	**Mushroom**	**Present work**

References

(1) Demas, J. N.; Crosby, G. A. Measurement of Photoluminescence Quantum Yields. Review. *J. Phys. Chem.* **1971**, *75* (8), 991–1024. https://doi.org/10.1021/J100678A001.

(2) Reichardt, C. Solvatochromic Dyes as Solvent Polarity Indicators. *Chem. Rev.* **1994**, *94* (8), 2319–2358. https://doi.org/10.1021/CR00032A005/ASSET/CR00032A005.FP.PNG_V03.

(3) Abbasi-Moayed, S.; Bigdeli, A.; Hormozi-Nezhad, M. R. Determination of Spermine and Spermidine in Meat with a Ratiometric Fluorescence Nanoprobe and a Combinational Logic Gate. *Food Chem.* **2022**, *384*, 132459. https://doi.org/10.1016/j.foodchem.2022.132459.

(4) Barros, M.; López-Carrasco, A.; Amorós, P.; Gil, S.; Gaviña, P.; Parra, M.; Haskouri, J. El; Terencio, M. C.; Costero, A. M. Chromogenic Chemodosimeter Based on Capped Silica Particles to Detect Spermine and Spermidine. *Nanomater. 2021, Vol. 11,* **2021**, *11* (3). https://doi.org/10.3390/nano11030818.

(5) Barros, M.; Ceballos, S.; Arroyo, P.; Sáez, J. A.; Parra, M.; Gil, S.; Costero, A. M.; Gaviña, P. Spermine and Spermidine Detection through Restricted Intramolecular Rotations in a Tetraphenylethylene Derivative. *Chemosens. 2022, Vol. 10,* **2021**, *10* (1). https://doi.org/10.3390/chemosensors10010008.

(6) Zhang, W.; Ma, J.; Sun, D. W.; Cheng, J.; Wang, Z.; Tang, B. Z. An Improved Ratiometric Fluorescent Tag Based on Aggregation-Induced Emission Luminogen for in-Situ Monitoring of Seafood Freshness. *Sensors Actuators B Chem.* **2022**, *373* (14), 132744. https://doi.org/10.1016/j.snb.2022.132744.

(7) Shi, Z.; Wu, Y.; Zhang, X.; Gao, Y.; Qiao, L.; Hou, Q.; Wang, M. Highly Sensitive and Selective Colorimetric and Fluorescent Dual-Readout Assay for the Analysis of Spermine, Spermidine and Cysteine. *Dye. Pigment.* **2023**, *220*, 111659. https://doi.org/10.1016/j.dyepig.2023.111659.

(8) Singh, P.; Sharma, P.; Sharma, N.; Kaur, S. Visual Detection of Spermine (Vapor and Aqueous Phase) in Food and Urine Samples: Bioimaging of Spermine in HeLa Cells. *Microchem. J.* **2022**, *183* (15), 108004. https://doi.org/10.1016/j.microc.2022.108004.

(9) Yang, Q.; Bai, Q.; Li, M.; Xiao, X. A Highly Sensitive Fluorescent Indicator Probe Based on Tetramethylcucurbit[6]Uril for Visual Detection of Spermine and Spermidine. *Microchem. J.* **2025**, *217* (30), 114840. https://doi.org/10.1016/j.microc.2025.114840.

(10) Stojanović, Z. S.; Đurović, A. D.; Kravić, S.; Ashrafi, A. M.; Richtera, L. Electrochemical Sensing Platform Based on the Use of ZnONPs and MWCNTs as CPE Modifiers for a Selective and Sensitive Determination of Polyamine Spermine in the Urine Sample. *Electroanalysis* **2023**, *35* (6), e202200446. https://doi.org/10.1002/elan.202200446.